# Electronically coupled complementary interfaces between perovskite band insulators

MARK HUIJBEN[1], GUUS RIJNDERS[1], DAVE H. A. BLANK[1]*, SARA BALS[2], SANDRA VAN AERT[2], JO VERBEECK[2], GUSTAAF VAN TENDELOO[2], ALEXANDER BRINKMAN[1] AND HANS HILGENKAMP[1]

[1]Faculty of Science & Technology and MESA+ Institute for Nanotechnology, University of Twente, PO Box 217, 7500 AE Enschede, The Netherlands
[2]Electron Microscopy for Materials Research (EMAT), University of Antwerp, Groenenborgerlaan 171, 2020 Antwerp, Belgium
*e-mail: d.h.a.blank@utwente.nl

Published online: 18 June 2006; doi:10.1038/nmat1675

Perovskite oxides exhibit a plethora of exceptional properties, providing the basis for novel concepts of oxide-electronic devices. The interest in these materials is even extended by the remarkable characteristics of their interfaces. Studies on single epitaxial connections between the wide-bandgap insulators $LaAlO_3$ and $SrTiO_3$ have revealed them to be either high-mobility electron conductors or insulating, depending on the atomic stacking sequences. For device applications, as well as for a basic understanding of the interface conduction mechanism, it is important to investigate the electronic coupling of closely spaced complementary interfaces. Here we report the successful realization of such coupled interfaces in $SrTiO_3$–$LaAlO_3$ thin-film multilayer structures. We found a critical separation distance of six perovskite unit cell layers, corresponding to approximately 23 Å, below which a decrease of the interface conductivity and carrier density occurs. Interestingly, the high carrier mobilities characterizing the separate conducting interfaces are found to be maintained in coupled structures down to subnanometre interface spacing.

Perovskite oxides and structurally related compounds have attracted great interest in the development of oxide-electronic devices, as they consist of a broad range of electronic phases[1,2]. The perovskites are commonly described in terms of their cubic unit cells, with the generic formula $ABO_3$. For a given parent compound, a rich phase diagram is coloured-in by a substitution of the cations A or B, and/or a change in the oxygen stoichiometry. The ionic character of the chemical bonds and the consequent possibility of electronic reconstruction often render interfaces in these materials strongly electronically active. To understand this interface activity, it is instructive to describe the perovskites in terms of their constituting AO and $BO_2$ layering sequence. For example, whereas the two band-insulators $SrTiO_3$ and $LaAlO_3$ are seemingly similar, the SrO and $TiO_2$ layers are charge-neutral, whereas the charge states in the $LaAlO_3$ are $(LaO)^+$ and $(AlO_2)^-$, respectively. In heterostructures, the AO–$BO_2$ stacking sequence is maintained and consequently a polarity discontinuity arises at the $LaAlO_3$–$SrTiO_3$ interface. It has been shown by Ohtomo and Hwang[3] that owing to this, the LaO:$TiO_2$ interface becomes conducting, and it is suggested that the conduction is governed by electron transfer from $LaAlO_3$ into the $TiO_2$ bonds of the $SrTiO_3$. The complementary $AlO_2$:SrO interface, with the $AlO_2$ possibly acting as an electron acceptor, remained insulating[3]. Such conducting interfaces are analogous to two-dimensional electron (hole) gases in semiconductors, which find applications in for example, optoelectronic, high-power radiofrequency and magnetoelectronic devices[4]. There is great interest in the fundamental properties of electronically coupled two-dimensional electron gases placed very near to each other[5].

Until now the investigations on the $LaAlO_3$–$SrTiO_3$ interface conduction effects have concentrated on individual interfaces[3]. To study the electronic coupling of the complementary interfaces between these insulators, we fabricated high-quality multilayers in which a variable number of $LaAlO_3$ unit cell layers are stacked between $SrTiO_3$, and *vice versa*. The $LaAlO_3$–$SrTiO_3$

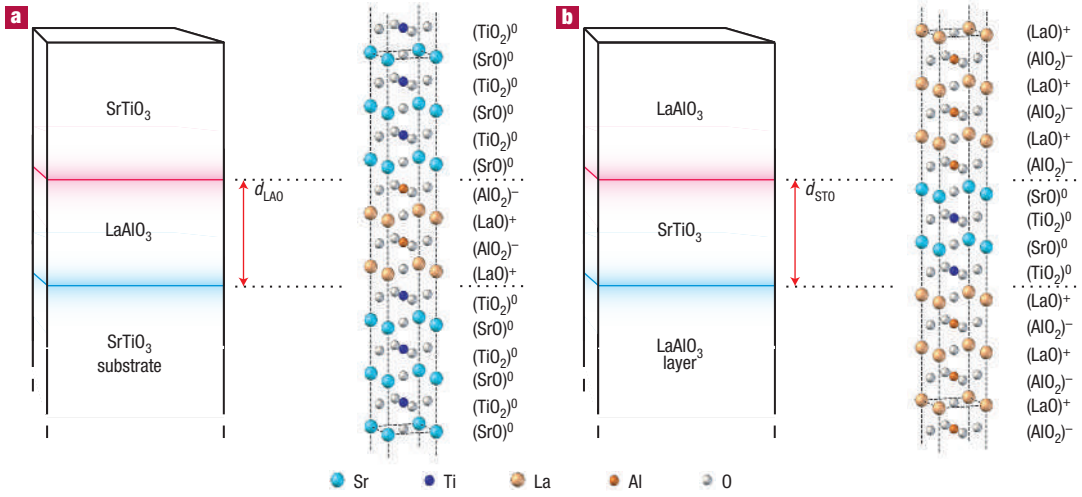


**Figure 1 Representation of the $LaAlO_3/SrTiO_3$ heterostructures investigated. a**, Schematic view of a $SrTiO_3/LaAlO_3/SrTiO_3$ heterostructure: a (001)-oriented $LaAlO_3/SrTiO_3$ bilayer grown on top of a $TiO_2$-terminated $SrTiO_3$ substrate, where the thickness of the $LaAlO_3$ layer ($d_{LAO}$) is varied. Atomic representation of the structure, here showing the composition and charge state of each layer for $d_{LAO} = 2$ unit cells. **b**, Schematic view of a $LaAlO_3/SrTiO_3/LaAlO_3$ heterostructure: a (001)-oriented $LaAlO_3/SrTiO_3/LaAlO_3$ trilayer grown on top of a SrO-terminated $SrTiO_3$ substrate, where the thickness of the $SrTiO_3$ layer ($d_{STO}$) is varied. Atomic representation of the structure, here showing the composition and charge state of each layer for $d_{STO} = 2$ unit cells.

heterostructures were grown by pulsed laser deposition, including *in situ* monitoring by reflective high-energy electron diffraction[6]. Single-crystal $LaAlO_3$ and $SrTiO_3$ targets have been used, applying a KrF excimer laser at a repetition rate of 1 Hz and a laser fluency of $\sim 1.3\,J\,cm^{-2}$. The deposition temperature was 850 °C, and the oxygen pressure was $3 \times 10^{-5}$ mbar.

The first type of heterostructure was deposited on $TiO_2$-terminated $SrTiO_3$ (100) substrates[7] and consisted of a $LaAlO_3$ layer followed by a $SrTiO_3$ top layer (Fig. 1a). Reflective high-energy electron-diffraction intensity oscillations were used to control the number of unit cell layers for both materials. The thickness of the $LaAlO_3$ layer was varied from 1 to 26 unit cells, whereas the number of unit cells for the $SrTiO_3$ top layer was always kept constant at 10. As the internal polarization of the $LaAlO_3$ is the driver for the interface doping, a change of the $LaAlO_3$ layer thickness could possibly result in a modification of this polarization. For this reason we have also fabricated heterostructures of a second type, in which a thin $SrTiO_3$ layer is sandwiched between sufficiently thick $LaAlO_3$ layers (Fig. 1b). For the fabrication of those heterostructures, the $TiO_2$-terminated $SrTiO_3$ (100) substrates were first covered with one monolayer of SrO by pulsed laser interval deposition[8] at 50 Hz. Subsequently, a $LaAlO_3$ base layer of 13 unit cells was deposited, followed by a $SrTiO_3$ layer, of which the thickness was varied from 2 to 11 unit cells, and finished by a $LaAlO_3$ top layer of 13 unit cells. Atomic force microscopy of the completed heterostructures showed atomically smooth terraces separated by unit cell steps, similar to the original substrate surface.

To examine the atomic stacking sequence at the interfaces, a superlattice of $LaAlO_3$ and $SrTiO_3$ was grown on a $TiO_2$-terminated $SrTiO_3$ substrate. Figure 2a shows a high-angle annular dark-field image taken along the [001] zone axis. In this image, which was obtained using a Titan 80-300 (FEI) scanning transmission electron microscope, the intensities of the atomic columns scale with the atomic number $Z$. The weaker TiO and AlO columns are located in the centre between the brighter Sr and La columns, respectively. To investigate the atomic layers at the interface (for example, $AlO_2$:SrO or LaO:$TiO_2$) the signal-to-noise ratio is increased by averaging over the area indicated by the white rectangle in Fig. 2a. This part of the image is divided into smaller subsections, which are added after cross correlation in Fig. 2b. To quantitatively evaluate the peak heights of the atom columns, statistical parameter estimation is used, in which a parametric model of gaussian peaks is fitted to Fig. 2b in the least-squares sense. Figure 2c,d shows the estimated peak heights corresponding to the La, Sr, TiO, and AlO columns and the atom columns ($X_A$, $X_B$) at both interfaces (indicated in Fig. 2b). The 90% confidence intervals have also been computed using the so-called Cramér–Rao lower bound[9]. Comparing the confidence intervals corresponding to the peak height of the atom columns at the interfaces with those of the surrounding TiO/AlO peaks confirms that the interface on top of every $SrTiO_3$ layer is $TiO_2$:LaO, whereas at the bottom it is $AlO_2$:SrO. These configurations are also expected from the deposition parameters. Recently Nakagawa *et al.*[10] found that interdiffusion of atoms at the interface only influenced the La/Sr sites with minimum influence on the Ti/Al stacking arrangement.

The electronic properties of the heterostructures were investigated by a four-point Van der Pauw method. For this, wire-bonded contacts were applied at the corners of the samples, connecting to the $(AlO_2)^-/(SrO)^0$ interface as well as to the $(LaO)^+/(TiO_2)^0$ interface. Measurements on individual interfaces using single $LaAlO_3$ layers on $SrTiO_3$ substrates confirmed the electron conduction of the $(LaO)^+/(TiO_2)^0$ interface with a sheet conductance of $1.4 \times 10^{-4}$ $(\Omega/\square)^{-1}$ at room temperature, whereas the $(AlO_2)^-/(SrO)^0$ interface had a sheet conductance of $\sim 10^{-7}\,(\Omega/\square)^{-1}$. The difference in sheet conductance between both types of interfaces is at least three orders of magnitude over the entire temperature range. All single interface experiments showed photoconductivity due to photocarrier injection. Ultraviolet light illumination on single $LaAlO_3$ layers on $SrTiO_3$ substrates increased the conductivity by factors of 2 and 120 for the $(LaO)^+/(TiO_2)^0$ and $(AlO_2)^-/(SrO)^0$ interfaces, respectively. Conductance enhancements were only observed for wavelengths of the illuminated light below 380 nm, corresponding to the bandgap of 3.2 eV of $SrTiO_3$. To enable a careful analysis of the

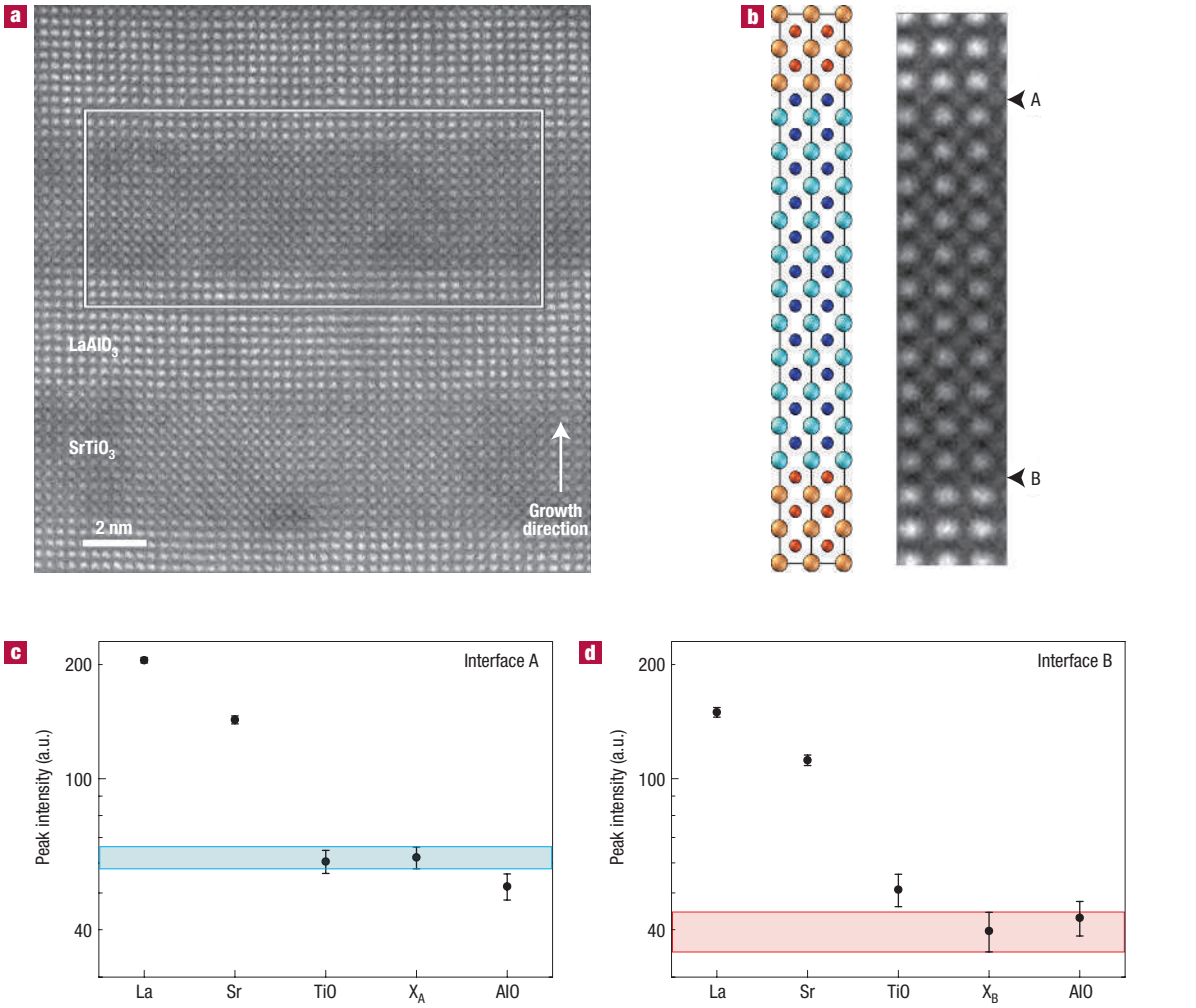


**Figure 2 Quantitative scanning transmission electron microscopy analysis of the atomic stacking sequences at the interfaces. a**, High-angle annular dark-field image of the $LaAlO_3/SrTiO_3$ superlattice along the [001] zone axis. The area of the image indicated by the white rectangle is used for averaging. **b**, Image showing the result of the averaging procedure, together with the atomic representation of the structure. The atomic positions are indicated in the same size and colour as in Fig. 1. The image is used as a starting point for quantitative peak estimation of the La, Sr, TiO and AlO columns and of the atom columns at the interfaces (indicated with A and B). **c**,**d**, The estimated peak heights of the La, Sr, TiO and AlO columns and of the atom columns at the interfaces (indicated with symbols $X_A$ and $X_B$) together with the corresponding 90% confidence intervals. The coloured bands indicate the 90% confidence intervals of the atom columns at the interfaces ($X_A$ and $X_B$).

intrinsic interface coupling, the effects of photocarrier injection were suppressed in the multilayer studies by shielding the samples from any light during the experiments and the 24 h before.

The sheet resistances $R_s$ at room temperature, for both types of heterostructures, are presented in Fig. 3a for different values of the separation distance ($d$) between the two interfaces. A decrease in $d$ is found to be accompanied by an increase in $R_s$ below a separation distance of six unit cells, corresponding to 23 Å. Interestingly, both types of heterostructures show a similar dependence on the interface separation distance, albeit with a difference of 20% in the absolute value of $R_s$. The sheet carrier densities $n_s$ were deduced from measurements of the Hall coefficient $R_H$, using $n_s = -1/R_H e$. The room-temperature results are shown in Fig. 3b. Below a separation distance of six unit cells a decrease in sheet carrier density occurs for both types of heterostructures. The constant $n_s$ for large $d$ has a value of $\sim 1.8 \times 10^{14}\,cm^{-2}$, corresponding to a charge density of $\sim 29\,\mu C\,cm^{-2}$, which is ~0.27 electrons per unit cell area on the $(LaO)^+/(TiO_2)^0$ interface. In this, the contribution by the $(AlO_2)^-/(SrO)^0$ interface to the carrier density is neglected, owing to its much lower conductivity. Recent studies demonstrate that the oxygen reduction of $SrTiO_3$ at very low deposition pressures ($<10^{-6}$ mbar)[11,12] induces sheet carrier densities in the order of $10^{16}-10^{17}\,cm^{-2}$. The role of oxygen vacancies in the creation of charge carriers is found to be negligible in our case, because of the high deposition pressure ($3 \times 10^{-5}$ mbar).

The change in $n_s$ and $R_s$ below a certain interface separation distance relates to the charge distribution in the heterostructure. To our knowledge, no theoretical modelling of the $SrTiO_3-LaAlO_3$ interface has been done, but it is interesting to make the comparison with interfaces between the Mott insulator $LaTiO_3$ and the band insulator[13–15] $SrTiO_3$. Notably, for that system a characteristic distance of six unit cells was predicted, over which charge transfer and electronic reconstruction takes place[14,15]. The electronic reconstruction at a $SrTiO_3-LaTiO_3$ interface creates partially filled Ti-3$d$ bands by band-bending effects, and the symmetric confinement of charge leads to a suppression of $n_s$. An

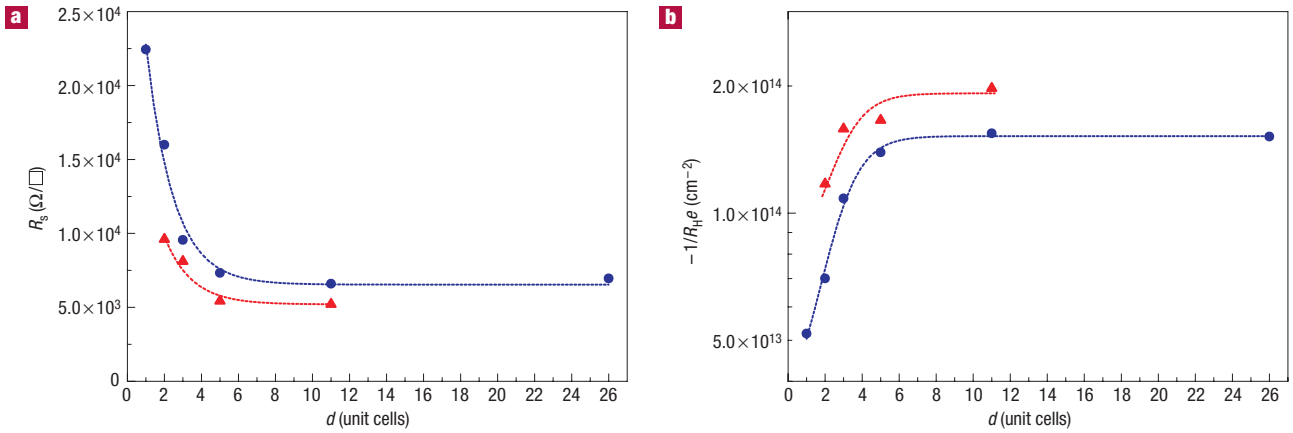


**Figure 3 Electronic properties of the $LaAlO_3/SrTiO_3$ heterostructures at 300 K for different separation distances between the interfaces. a**, Dependence of the sheet resistance $R_s$ on the separation distance $d$. **b**, Dependence of $-1/R_H e$ on the separation distance $d$. $SrTiO_3/LaAlO_3/SrTiO_3$ heterostructures and $LaAlO_3/SrTiO_3/LaAlO_3$ heterostructures are indicated by circles and triangles, respectively. The dashed lines are guides to the eye.

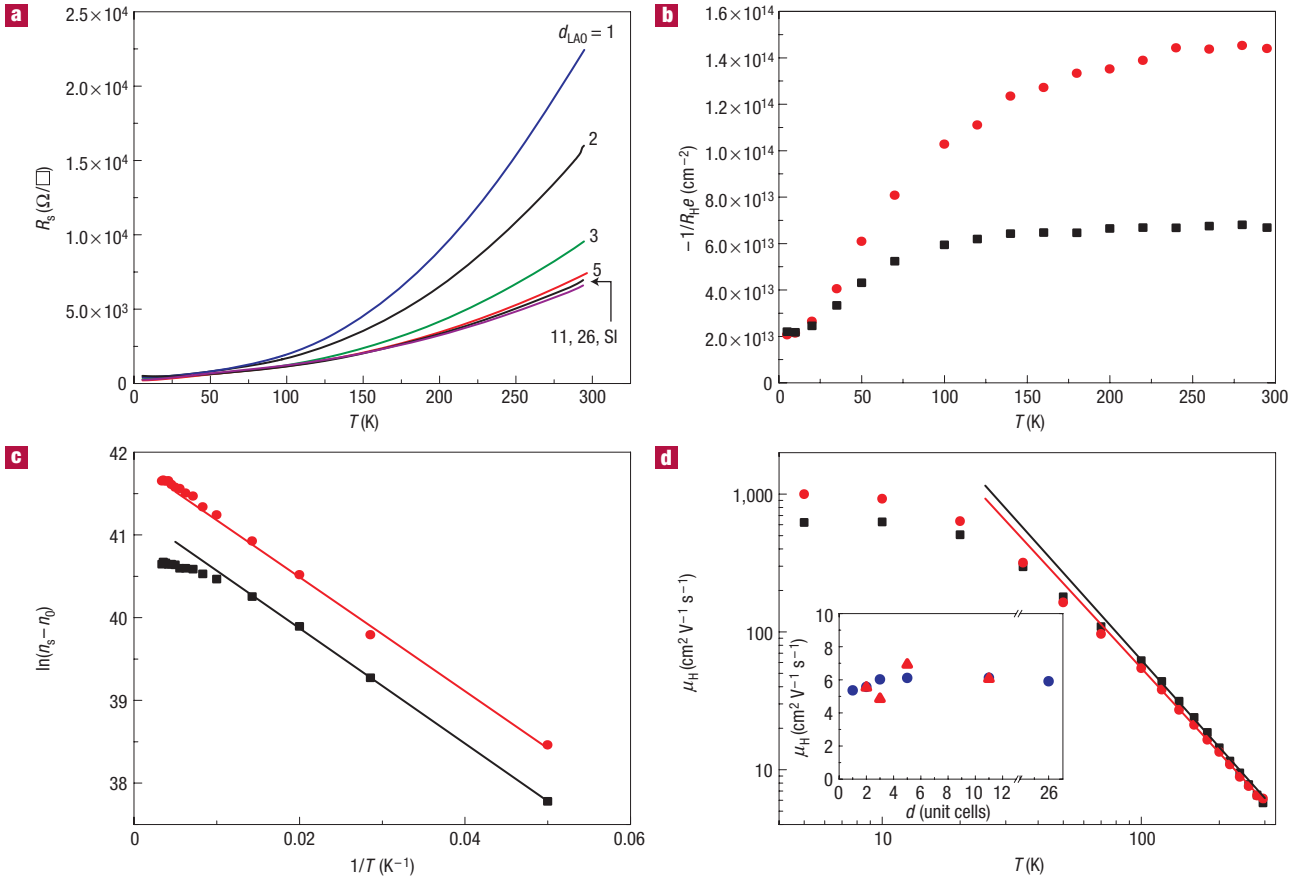


**Figure 4 Transport properties of the $LaAlO_3/SrTiO_3$ heterostructures for different separation distances between the interfaces. a**, The temperature dependence of the sheet resistance $R_s(T)$ for different thicknesses of the $LaAlO_3$ layer ($d_{LAO}$) in $SrTiO_3/LaAlO_3/SrTiO_3$ heterostructures. A measurement on a single $(LaO)^+/(TiO_2)^0$ interface (SI) is also indicated. **b**, Temperature dependence of $-1/R_H e(T)$ for $SrTiO_3/LaAlO_3/SrTiO_3$ heterostructures with separation distances of $d_{LAO} = 2$ (squares) and 5 (circles) unit cells. **c**, Temperature dependence of $\ln(n_s - n_0)$ for $SrTiO_3/LaAlO_3/SrTiO_3$ heterostructures with separation distances of $d_{LAO} = 2$ (squares) and 5 (circles) unit cells, where $n_s$ is defined as $-1/R_H e$ and $n_0$ is the low-temperature limit of $n_s$. **d**, Temperature dependence of Hall mobility $\mu_H(T)$ for $SrTiO_3/LaAlO_3/SrTiO_3$ heterostructures with separation distances of $d_{LAO} = 2$ (squares) and 5 (circles) unit cells. The inset shows the separation distance $d$ dependence of $\mu_H(T)$ at 300K, where $SrTiO_3/LaAlO_3/SrTiO_3$ heterostructures and $LaAlO_3/SrTiO_3/LaAlO_3$ heterostructures are indicated by circles and triangles, respectively.

important difference with our experiments is the absence of $TiO_2$ layers in parts of our heterostructures. At the $LaAlO_3$ side, subbands are possibly created below the La-5*d* levels, in analogy with the Ti-3*d* levels at the $SrTiO_3$ side. The suppression of $n_s$, induced by the coupling between the interfaces, could then result from the constraint that the charge density at the $(AlO_2)^-/(SrO)^0$ interface is low.

The temperature dependence of the sheet resistance and the Hall coefficient provides further insight into the electronic properties of the interface electron gas. For the $SrTiO_3/LaAlO_3/SrTiO_3$ heterostructures, the temperature dependence of the sheet resistance $R_s(T)$ is shown in Fig. 4a for different values of the $LaAlO_3$ layer thickness ($d_{LAO}$), and Fig. 4b shows the carrier density as determined from the Hall effect as a function of temperature. The energy scale over which charge carriers seem to be frozen out is 6.0 meV (Fig. 4c), which is comparable to observations in $SrTiO_3$ at low La doping[16]. At temperatures above 100 K, the carrier density for $d_{LAO} = 2$ unit cells is approximately constant, for $d_{LAO} = 5$ unit cells the thermally activated increase continues.

The temperature dependence of the Hall mobility $\mu_H$ is given in Fig. 4d. Above 50 K the mobilities show a $T^{-2}$ power-law dependence, characteristic of Fermi-liquid behaviour. Electron–phonon interactions are typically weak in $SrTiO_3$ (as is known from the poor heat conduction) and would give rise to a Bloch–Grüneisen temperature dependence of the resistance, which is not observed. Although electron–electron scattering is typically suppressed by screening and the Pauli exclusion principle, it is known to be relevant in transition metals with partially filled *d*-shells. At the LaO–$TiO_2$ interface, this effect is expected to be important if interface electronic reconstruction makes the Fermi surface intersect the Ti-3*d* subbands[14,15,17]. In addition, it is known that other effects, such as disorder, can give rise to $T^{-2}$ temperature dependencies. For all heterostructures, $\mu_H$ at room temperature is found to be constant at $6.0 \pm 1.0\,cm^2\,V^{-1}\,s^{-1}$, without any dependence on the separation distances ($d_{LAO}$ and $d_{STO}$). This value corresponds with room-temperature mobilities reported for single interfaces[3,18]. The very large mobilities in the zero-temperature limit provide an estimated electronic mean free path of 100 nm–1 μm. This large electronic mean free path and the fact that $\mu_H$ does not decrease for decreasing interlayer thickness indicates that electron scattering at impurities or crystalline defects in the nearby interface are not dominating effects for the mobilities at room temperature.

These studies on the $LaAlO_3$:$SrTiO_3$ heterostructures prove the possibility to realize closely spaced conducting sheets in these otherwise insulating oxide systems. This provides a perspective for novel all-oxide electronic devices as well as for basic studies. In this respect it is interesting to note that the growth techniques used can also be applied to the fabrication of multilayers with exclusively electron-doped LaO–$TiO_2$ interfaces, by combining the $SrTiO_3$ and $LaAlO_3$ layers with single layers of $LaTiO_3$ or $TiO_2$.

Received 21 March 2006; accepted 19 May 2006; published 18 June 2006.

## References


1. Ahn, C. H., Triscone, J. M. & Mannhart, J. Electric field effect in correlated oxide systems. *Nature* **424,** 1015–1018 (2003).
2. Dagotto, E. Complexity in strongly correlated electron systems. *Science* **309,** 257–262 (2005).
3. Ohtomo, A. & Hwang, H. Y. A high-mobility electron gas at the $LaAlO_3/SrTiO_3$ heterointerface. *Nature* **427,** 423–426 (2004).
4. Ando, T., Fowler, A. B. & Stern, F. Electronic properties of two-dimensional systems. *Rev. Mod. Phys.* **54,** 437–672 (1982).
5. Eisenstein, J. P. & MacDonald, A. H. Bose–Einstein condensation of excitons in bilayer electron systems. *Nature* **432,** 691–694 (2004).
6. Rijnders, G. J. H. M., Koster, G., Blank, D. H. A. & Rogalla, H. In situ monitoring during pulsed laser deposition of complex oxides using reflection high-energy electron diffraction under high oxygen pressure. *Appl. Phys. Lett.* **70,** 1888–1890 (1997).
7. Koster, G., Kropman, B. L., Rijnders, G. J. H. M., Blank, D. H. A. & Rogalla, H. Quasi-ideal strontium titanate crystal surfaces through formation of strontium hydroxide. *Appl. Phys. Lett.* **73,** 2920–2922 (1998).
8. Koster, G., Rijnders, G. J. H. M., Blank, D. H. A. & Rogalla, H. Imposed layer-by-layer growth by pulsed laser interval deposition. *Appl. Phys. Lett.* **74,** 3729–3731 (1999).
9. Den Dekker, A. J., Van Aert, S., Van den Bos, A. & Van Dyck, D. Maximum likelihood estimation of structure parameters from high resolution electron microscopy images. Part I: A theoretical framework. *Ultramicroscopy* **104,** 83–106 (2005).
10. Nakagawa, N., Hwang, H. Y. & Muller, D. A. Why some interfaces cannot be sharp. *Nature Mater.* **5,** 204–209 (2006).
11. Kalabukhov, A. S. *et al.* The role of oxygen vacancies in $SrTiO_3$ at the $LaAlO_3/SrTiO_3$ interface. Preprint at <http://arxiv.org/abs/cond-mat/0603501> (2006).
12. Siemons, W. *et al.* Origin of the unusual transport properties observed at hetero-interfaces of $LaAlO_3$ on $SrTiO_3$. Preprint at <http://arxiv.org/abs/cond-mat/0603598> (2006).
13. Ohtomo, A., Muller, D. A., Grazul, J. L. & Hwang, H. Y. Artificial charge-modulation in atomic-scale perovskite titanate superlattices. *Nature* **419,** 378–380 (2002).
14. Okamoto, S. & Millis, A. J. Electronic reconstruction at an interface between a Mott insulator and a band insulator. *Nature* **428,** 630–633 (2004).
15. Okamoto, S. & Millis, A. J. Theory of Mott insulator-band insulator heterostructures. *Phys. Rev. B* **70,** 075101 (2004).
16. Okuda, T., Nakanishi, K., Miyasaka, S. & Tokura, Y. Large thermoelectric response of metallic perovskites: $Sr_{1-x}La_xTiO_3$ ($0 \le x \le 0.1$). *Phys. Rev. B* **63,** 113104 (2001).
17. Henrich, V. E., Dresselhaus, G. & Zeiger, H. J. Surface defects and the electronic structure of $SrTiO_3$ surfaces. *Phys. Rev. B* **17,** 4908–4921 (1987).
18. Nishimura, J., Ohtomo, A., Ohkubo, A., Murakami, Y. & Kawasaki, M. Controlled carrier generation at a polarity-discontinued perovskite heterointerface. *Jpn J. Appl. Phys.* **43,** L1032–L1034 (2004).


## Acknowledgements

This work is part of the research programme of the Foundation for Fundamental Research on Matter (FOM, financially supported by the Netherlands Organisation for Scientific Research (NWO)) and Philips Research. A.B., D.H.A.B., H.H. and G.R. acknowledge additional support from NWO. S.B. and S.V.A. are grateful to the Fund for Scientific Research-Flanders. The authors also acknowledge B. Freitag, A. J. Millis, Y. Ponomarev, F. J. G. Roesthuis, H. Rogalla, R. Wolters, W. van der Wiel, D. Veldhuis and the FEI Company.
Correspondence and requests for materials should be addressed to D.H.A.B.

## Competing financial interests

The authors declare that they have no competing financial interests.